Comparative analysis of microclimate simulations

Assessing the single-layer urban canopy model and ENVI-met in Hong Kong

Lieber, Jonathan; Chen, Xuan; Chen, Liutao; Yang, Jiachuan

DOI
10.1016/j.uclim.2025.102621

Publication date
2025

Document Version
Final published version

Published in
Urban Climate

Urban Climate 64 (2025) 102621

Contents lists available at ScienceDirect

Urban Climate

journal homepage: www.elsevier.com/locate/uclim

Comparative analysis of microclimate simulations: Assessing the single-layer urban canopy model and ENVI-met in Hong Kong

Jonathan Lieber [a], Xuan Chen [b], Liutao Chen [a], Jiachuan Yang [a,*]

[a] Department of Civil and Environmental Engineering, The Hong Kong University of Science and Technology, Hong Kong, China
[b] Department of Water Management, Faculty of Civil Engineering and Geosciences, Delft University of Technology, Delft, the Netherlands

ARTICLE INFO

Keywords:
Urban climate modeling
Single-layer urban canopy model (SLUCM)
ENVI-met
Urban heat island

ABSTRACT

As global warming and urban overheating continue to intensify, accurate urban microclimate modeling has become critical for sustainable urban planning. While the Single-layer urban canopy model (SLUCM, a reduced-order surface energy balance model) and ENVI-met (a computational fluid dynamic model) are the two most widely used models, a direct comparison of their performance is missing. This study aims to examine potential biases between SLUCM and ENVI-met using Hong Kong as a case study and provide guidance on model selection for different purposes. Evaluated against pedestrian-level observational data, the results show that both SLUCM and ENVI-met simulate air temperatures reasonably well, with mean absolute errors less than 1.5 °C. However, SLUCM outperforms ENVI-met in simulating relative humidity, which is partially caused by the insufficient representation of sea breeze by both models. To extrapolate SLUCM output to different heights, Monin-Obukhov similarity theory is applied. This leads to large gradient of temperature and humidity in the vertical direction, while ENVI-met simulations yield homogeneous profiles due to explicit modeling of the turbulent mixing. Findings suggest that ENVI-met suits heterogeneous neighborhoods where turbulent mixing is largely regulated by urban morphology, but its accuracy on humidity simulation needs special attention. SLUCM performs reasonably well in simulating air temperature, but it tends to yield large bias in the vertical direction. Based on the findings, we recommend development of enhanced turbulence parameterization for SLUCM, and coupling both models with mesoscale models to better account for the effect of land/sea breeze on urban microclimate in coastal cities.

1. Introduction

As global urbanization accelerates, the urban population has surged from 734.5 million in 1950 to 4.09 billion in 2018, with projections estimating it will reach 6.68 billion by 2050 (Ritchie et al., 2018). This rapid growth has made the management of urban

Acronym: AUS, Austin road (study site); BEM, Building energy model; CFD, Computational fluid dynamics; CoWIN, Community Weather Information Network; HOL, Hollywood road (study site); LCZ, Local climate zone; MAE, Mean absolute error; MOST, Monin-Obukhov similarity theory; NAT, Nathan road (study site); RH, Relative humidity; $RH_{1.5}$, Relative humidity at a height of 1.5 m; RH2, Relative humidity at a height of 2 m; RH_{can}, Mean relative humidity of the canyon; SEB, Surface energy balance; SLUCM, Single layer urban canopy model; Ta, Air temperature; $T_{1.5}$, Air temperature at a height of 1.5 m; T_2, Air temperature at a height of 2 m; T_{can}, Mean air temperature of the canyon; TKE, Turbulent kinetic energy; UCM, Urban canopy model; WRF, Weather Research and Forecasting model.

* Corresponding author.
E-mail address: cejcyang@ust.hk (J. Yang).

https://doi.org/10.1016/j.uclim.2025.102621
Received 6 December 2024; Received in revised form 16 July 2025; Accepted 15 September 2025
Available online 26 September 2025

thermal environments critical for protecting public health and enhancing urban resilience (Fu et al., 2024). Urbanization significantly alters thermal dynamics in cities by increasing radiation absorption, reducing evapotranspiration, and decreasing surface albedo, which collectively contribute to the elevated urban air temperatures (T_a) (Oke, 1982). This phenomenon, known as the urban heat island effect, is compounded by stagnant winds, air pollution, and climate change (Singh et al., 2020). The resulting magnitude of the effect poses increased risks to vulnerable populations and urban infrastructure (European Commission, 2018). For example, Laaidi et al. (2012) demonstrated that prolonged exposure to high nighttime T_a significantly increased mortality risk among elderly individuals in urban settings during heat waves.

The development of urban climate models is essential for predicting thermal challenges and mitigating associated risks. Traditionally, climate models have been applied at global (10,000 km – 1000 km) or meso-scale (1000 km - 10 km) levels; however, advancements in computational capabilities have enabled modeling at high spatial resolutions, extending to the local (10 km - 1 km) and microscale (< 1 km) (Oke et al., 2017). Two prominent types of microclimate models are surface energy balance (SEB) and computational fluid dynamics (CFD) models (Hidalgo et al., 2008). Both types of models adopt meteorological forcing from the lowest atmosphere level to drive simulations and emphasize the influence of urban landscape and anthropogenic activities on urban microclimate (Zhao et al., 2021). The importance of micro-scale modeling lies in the significant intra-city variations compared to inter-city difference. For instance, Cao et al. (2022) demonstrated that the variability of nighttime T_a at a height of 2 m (T_2) can differ by as much as 2.5 °C across various local climate zones (LCZ) within a single city. Based on the review study by Krayenhoff et al. (2021), the most representative numerical tools in the literature for urban microclimate modeling are ENVI-met and the Single-layer Urban Canopy Model (SLUCM).

ENVI-met excels in simulating urban microclimate by explicitly representing the buildings, vegetation, and incoming flow in a 3D environment (Tsoka et al., 2018). This model uses a CFD approach that relies on Reynolds-averaged Navier–Stokes equations to solve the exchange of energy, mass, and momentum in the built environment. ENVI-met is particularly effective in analyzing small-scale urban elements and their microclimatic impacts, such as street trees, green roof (Huttner, 2012). Key strengths of ENVI-met include its detailed representation of surface-plant-air interactions, encompassing processes such as shading, evapotranspiration, and turbulent flow dynamics (Ozkeresteci et al., 2003). However, ENVI-met can be computationally demanding as it requires short time steps (typically 30 mins) and fine-grid resolution (generally 2 m) to maximize simulation accuracy (Forouzandeh, 2021). Furthermore, the proprietary nature of ENVI-met limits access to the source code, resulting in reduced transparency regarding the underlying algorithms and equations (Crank et al., 2020). On the other hand, SLUCM is a type of surface energy balance model that focuses on solving energy and moisture exchanges within the canopy layer (Kusaka et al., 2001). It is designed to handle local to regional scale urban areas, e.g., simulating the effect of heat island mitigation strategies at the range of 0.1–10 km (Yang et al., 2016). SLUCM simulates urban areas as 2D long canyons with buildings of equal height on both sides of the street. With this treatment, radiative exchange and wind flow in 3D environment can be largely simplified that SLUCM features a low computational cost. Compared to ENVI-met, SLUCM's physics are more clearly defined with supporting references in the literature, making it easier to understand and modify, as detailed in the foundational work of Kusaka et al. (2001). However, SLUCM may not capture microscale processes as accurately as ENVI-met due to the parameterization of wind flow (Afshari and Ramirez, 2021; Conigliaro et al., 2021; Eingrüber and Scherer, 2023).

Numerous studies have validated SLUCM and ENVI-met by comparing their simulations with observational data. For example, Li et al. (2019) evaluated the SLUCM coupled with the WRF model in simulating urban climate of the Pearl River Delta, China. They found good simulations of T_2 with an annual mean Perkins Skill Score of 0.724. Tsoka et al. (2018) reviewed ENVI-met's performance across multiple studies, and suggested it generally captures the T_a diurnal cycles well with low median errors for T_a (MAE of 1.34 °C). For relative humidity (RH), ten studies reported MAE ranging from 2.50 % to 7.78 %, with higher errors in areas influenced by sea breezes (Tsoka et al., 2018). After evaluating model's accuracy, both ENVI-met and SLUCM offer a cost-effective approach to tackle climate-related challenges in urban areas without the need for costly trial-and-error iterations in real applications. For instance, Cortes et al. (2022) utilized ENVI-met to simulate the microclimate effects of increasing vegetation, adding open spaces, and employing green roofs in Mandaue City, Philippines. They demonstrated potential reductions in T_a by up to 0.4 °C. Similarly, Khan et al. (2022) utilized SLUCM to assess the impact of increased green infrastructure in Athens, Greece. Their findings suggested that expanding green cover by up to 70 % could decrease daytime summer T_a by 1.1 °C and nighttime T_a by 1.9 °C. With elevated heat stress in recent years, the accuracy of urban climate models like ENVI-met and SLUCM have become crucial to provide reliable scientific basis to support the development of heat mitigation strategies (Karlický et al., 2018). As each model has its own assumptions and parameterizations, it is expected that SLUCM and ENVI-met will have different performances under different conditions.

Despite the substantial number of urban microclimate simulation studies in the literature, comparative analyses of SLUCM and ENVI-met performance are largely missing. The lack of comparative analyses is likely caused by cross-disciplinary knowledge gap. SLUCM and other urban canopy models (UCM) are typically used in atmospheric science community focused on land-atmosphere interactions, while ENVI-met is usually adopted by architects and urban planners for microclimate design applications. Performance of UCMs is normally evaluated against in-situ measurement of sensible and latent heat fluxes (Lipson et al., 2024), while ENVI-met simulations are mainly validated against T_a data (Liu et al., 2021). Berardi et al. (2020) is among the few study that compared ENVI-met against UCM simulations. They reported a MAE of less than 0.5 °C for ENVI-met, and a MAE of 0.60–1.59 °C for multi-layer UCM in simulating urban T_a during heat wave periods in the Greater Toronto Area. Their study also revealed consistent predictions for urban greening impacts by UCM and ENVI-met, with UCM predicted cooling of 1.6–2.3 °C and ENVI-met predicted cooling of 0.5–1.4 °C. However, a meta-analysis conducted by Krayenhoff et al. (2021) summarized that the simulated cooling effect of roof albedo by SLUCM and ENVI-met can vary by an order of magnitude. Such large discrepancy in model results call for the need of a direct comparison between SLUCM and ENVI-met to examine potential biases between these two models, and consequently provide guidance

on model selection for different purposes.

To bridge this gap, this study aims to compare the performance of SLUCM and ENVI-met in simulating urban microclimate in Hong Kong. This comparison will facilitate a deeper understanding of the strengths, limitations, and potential applications of CFD and SEB approaches in simulating urban microclimate through these two widely used models. The findings will connect the atmospheric science community with architects and urban planners in microclimate research, and thus help researchers and practitioners better select appropriate models for their applications, as well as reveal opportunities for collaborative model enhancements. Specifically, the research questions addressed are:

1. How do SLUCM and ENVI-met compare in their evaluation against high resolution pedestrian-level observational data?
2. What are the differences in the diurnal and vertical profiles simulated by the two models?
3. Which physical processes and/or parametrization schemes in SLUCM and ENVI-met cause the difference in simulated microclimate?

This study employs LCZ classification to enable standardized urban climate analysis across different areas. LCZ is a land-use climate-oriented categorization system for urban landscapes based on their surface structure, material composition, and human activity, and ability to modify canopy T_a at a local scale (Stewart and Oke, 2012). The comparison is made against high resolution pedestrian-level observational data from three case studies within LCZ 1 urban street canyon in Hong Kong. We look into the diurnal and vertical profiles of simulated T_a and RH by SLUCM and ENVI-met to present a comprehensive evaluation on the capabilities and limitations of both models in simulating the variation of urban microclimate with height and time.

The paper is organized as follows: Section 2 describes the study area, measurement data, meteorological forcing, and model setup for both ENVI-met and SLUCM. Section 3 presents the model validation results, analysis of diurnal microclimate cycles, and vertical profiles of T_a and RH. Finally, Section 4 provides conclusions and recommendations.

2. Material and methods

2.1. Study area and measurement data

Three street canyon sites in Hong Kong were selected as study locations (Fig. 1a). Located on the southeastern coast of China, Hong Kong has a subtropical climate and is densely populated, with 6800 people per square kilometer (Government of Hong Kong, 2022). Between 1885 and 2008, Hong Kong experienced a significant shift in extreme T_a events, with overall T_a trends rising by 0.09 °C to 0.14 °C per decade (Lee et al., 2011). The number of very hot days and hot nights increased by 1.07 days and 1.51 nights per decade, respectively, while cold days decreased by 1.19 days per decade (Lee et al., 2011). Urban overheating poses significant risks to resident health and energy resilience in Hong Kong, making it a suitable place for evaluating urban microclimate models where accurate T_a simulation is crucial for heat mitigation and adaptation.

These sites are located along collection routes of previous mobile measurement studies (Chen et al., 2024a and hence have high resolution pedestrian-level observational data for model validation. The street canyons chosen, Nathan Road in Mong Kok (NAT), Austin Road in Tsim Sha Tsui (AUS), and Hollywood Road in Central (HOL), represent a diverse sample of one of the dominate LCZ types in Hong Kong: LCZ 1 - compact high-rise. In-land linear canyons with no vegetation were prioritized for selection to minimize coastal influences and replicate the simplified canyon assumptions used by the SLUCM model, which consists of an infinitely long 2D canyon with standardized building dimensions.

Microclimate observational data used for evaluating model performances in this study were sourced from (Chen et al., 2024a).

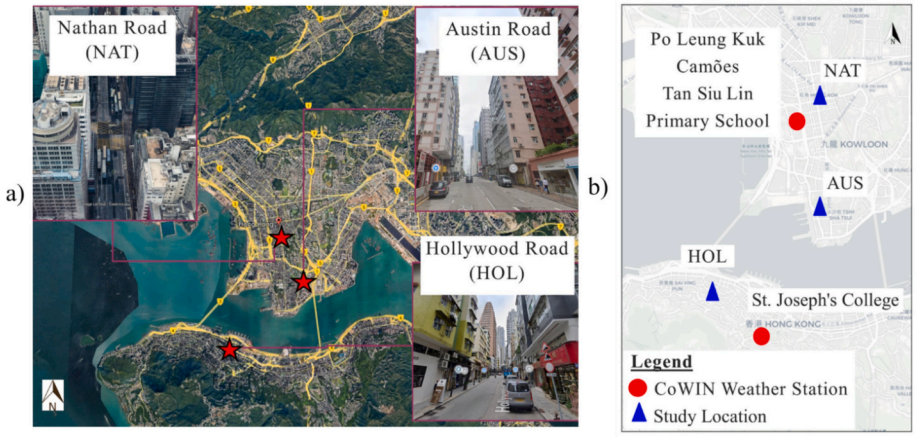

Fig. 1. Overview of the study sites in Hong Kong and their respective contexts. (a) Satellite imagery overlaid with street-level snapshots of the study locations: retrieved from Google Maps on January 21, 2023. (b) A map indicating the proximity of the study sites to CoWIN weather stations.

Chen et al. (2024a) conducted mobile field measurements on 8 days in Hong Kong during 2021 and 2022. The measurements were carried out on Sundays at 10:00, 14:00, and 19:00. Fig. 2a depicts one data collection route in Central, which covers the HOL site in this study (NAT and AUS sites are included in other routes not shown here). The Heat Stress WBGT Meter (TM-188/TM-188D) was used to gather T_a and RH with a sampling interval of 20 s along the route (Fig. 2b). Measurements were taken by walking with an approximate measurement height of 1.5 m. For validating the microclimate simulations by SLUCM and ENVI-met, observed T_a and RH at the height of 1.5 m over three study sites on September 12th, 2021 and October 17th, 2021 is used. Details of the measurement routes and data collection can be found in (Chen et al., 2024a).

2.2. Meteorological forcing

Meteorological forcing data were obtained from the Community Weather Information Network (CoWIN), which consists of a series of local weather stations managed by the University of Hong Kong and the Hong Kong Observatory (Community Weather Information Network, 2023). This network provides quality-controlled hourly averages of key variables such as T_a, RH, wind direction, and speed, collected on rooftops at a height of 16 to 20 m above the ground surface (Lam et al., 2021). Meteorological forcing data for each study site were sourced from the nearest CoWIN station (Fig. 1b). Specifically, the Po Leung Kuk Camões Tan Siu Lin Primary School station was closest to the NAT and AUS sites, while the St. Joseph's College station was nearest to the HOL site. To meet ENVI-met's requirement of 30-min interval forcing, the hourly data underwent interpolation using a method described by the Ernest Orlando Lawrence Berkeley National Laboratory (2014). In contrast to ENVI-met, SLUCM utilized hourly meteorological forcing data directly, obviating the need for temporal interpolation.

The simulations were conducted over two periods: September 11th–12th, 2021, and October 16th–17th, 2021, selected due to the availability of observational data. Simulations began at 00:00 to capture the full daily cycle of atmospheric conditions, as suggested by Salata et al. (2016). Each simulation spanned 48 h, with the final 24 h utilized for analysis purposes to ensure model stability after an initial spin-up phase of 24 h. While urban climatic studies often focus on hot summer conditions, Tsoka et al. (2018) argue that winter and intermediate seasons can also provide valuable insights. The hot September conditions (29 °C - 36 °C) and comparatively cooler October conditions (22 °C - 28 °C) of 2021 (Fig. 3a) represent diverse meteorological conditions. This allows us to better test the performance of the ENVI-met and SLUCM models.

2.3. ENVI-met setup

The configuration of the 3D ENVI-met model domains was based on urban morphological data sourced from the Common Spatial Data Infrastructure Portal of the Hong Kong Planning Department (CSDI, 2022). Consistent with methodologies applied in previous ENVI-met analyses within Hong Kong (Morakinyo et al., 2018), buildings within these domains were represented using lightweight concrete characterized by an albedo of 0.3, surrounded by asphalt roads. The model's spatial resolution was set at 2 m, covering an area of approximately 100–200 m by 100–300 m. Salvati and Kolokotroni (2019) reported that this scale generates more accurate simulations compared to larger model domains. The domains extended vertically to a height three times that of the tallest building, integrating 7 nesting grids to serve as a buffer zone. Full forcing was used under the assumption of clear skies, without cloud cover or precipitation, and a roughness length parameter was set at 0.1.

To understand the differences in simulated microclimate by ENVI-met and SLUCM, it is essential to recognize the main physical processes and parameterization schemes in both models (Table 1). ENVI-met employs the k-ε turbulence closure model to solve 3D Reynolds-averaged Navier–Stokes equations for airflow, capturing phenomena like wind tunneling around buildings (Tsoka et al., 2018; Masson et al., 2020). Its radiation scheme uses a multi-reflection ray-tracing method to compute shortwave and longwave fluxes per grid cell, accounting for shading and reflections in complex built environments (Simon et al., 2021). Turbulent heat fluxes are calculated based on the k-ε model, resolving sensible and latent heat exchanges explicitly through turbulent mixing and advection (ENVI-met, 2025c). Moisture transport is modeled explicitly, incorporating vegetation transpiration and soil evaporation (Ozkeresteci

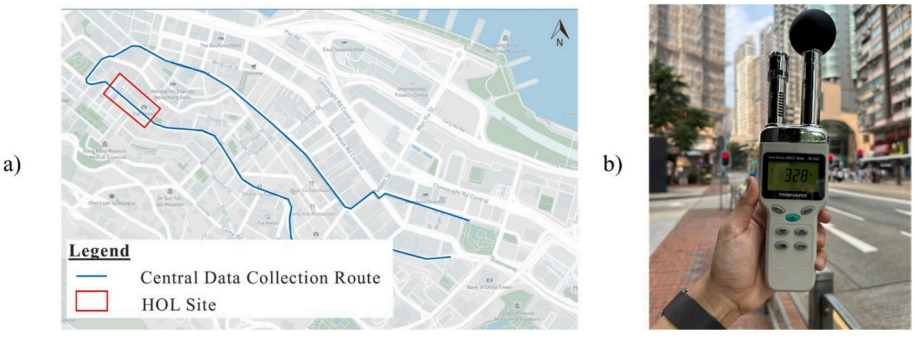

Fig. 2. (a) Microclimate observation route (blue line) in Central. The red rectangle denotes the HOL site in this study. (b) Heat Stress WBGT Meter used for data collection at a height of 1.5 m by Chen et al. (2024a). (For interpretation of the references to colour in this figure legend, the reader is referred to the web version of this article.)

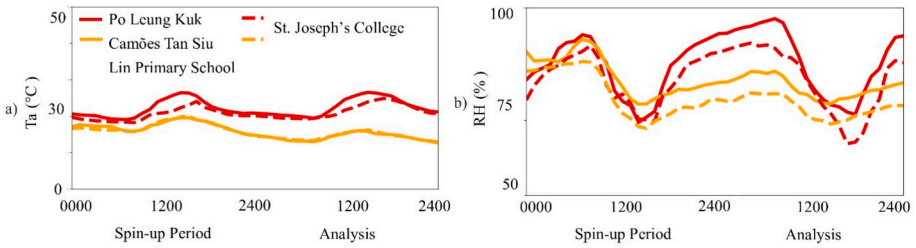

Fig. 3. Temporal variations of input (a) T_a (°C) and (b) RH (%) recorded by two CoWIN stations in Hong Kong on September 11–12, 2021 (red lines) and October 16–17, 2021 (orange lines). (For interpretation of the references to colour in this figure legend, the reader is referred to the web version of this article.)

Table 1
Summary of the setup and parameterization schemes used in the SLUCM and ENVI-met simulations.

Parameter	Value	Reference
Meteorological forcing data	Nearest CoWIN station	Community Weather Information Network (2023)
Building geometry	–	CSDI (2022)
Building and road material	Concrete buildings and asphalt roads	Morakinyo et al. (2017)
Material albedo	Lightweight concrete (0.3)	Morakinyo et al. (2020)
Simulation time	48 h (24 h Spin-up)	Di Giuseppe et al. (2021), Salata et al. (2016)
ENVI-met		
Radiative transfer	Multi-reflection ray-tracing method	ENVI-met (2025b)
Energy balance	Prognostic surface energy balance with detailed heat exchange processes	ENVI-met (2025b)
Wind flow	3D k-ε turbulence closure model with Reynolds-averaged Navier–Stokes equation	ENVI-met. (2025c)
Turbulent heat flux	Explicitly resolved via k-ε model for sensible and latent heat	ENVI-met. (2025c)
Anthropogenic heat	Not explicitly modeled	ENVI-met (2025a)
Domain size	Approx. 200 m × 200 m	Salvati and Kolokotroni (2019)
Cell resolution	2 m	Chatzinikolaou et al. (2018)
Material thermal conductivity	0.2 $W/(m \cdot K)$	
Material heat capacity	Wall: 1.3×10^6 $J/(K \cdot m^3)$ Roof: 1.3×10^6 $J/(K \cdot m^3)$	
Material absorption	0.7	
Material thickness	0.3 m	
Nesting grids	5–7 empty or nesting cells	Shinzato et al (2019), Di Giuseppe et al. (2021)
SLUCM		
Radiative transfer	Simplified radiation scheme with mean view factors	Kusaka et al. (2001), Kusaka and Kimura (2004)
Energy balance	Solved as a mean at individual urban surface	Kusaka et al. (2001), Kusaka and Kimura (2004)
Wind flow	Prescribed profiles: logarithmic above canyon and exponential within canyon	Kusaka et al. (2001), Kusaka and Kimura (2004),
Turbulent heat flux	Bulk aerodynamic resistance method	Kusaka et al. (2001), Kusaka and Kimura (2004)
Anthropogenic heat	Box-type BEM with heat flux added as bulk flux into the canyon	(Chen et al., 2021; Chen et al., 2024b)
Building type	Residential	–
Material thermal conductivity	Wall: 0.6 $W/(m \cdot K)$ Roof: 0.2 $W/(m \cdot K)$	–
Material heat capacity	Wall: 1.6×10^6 $J/(K \cdot m^3)$ Roof: 1.6×10^6 $J/(K \cdot m^3)$	–
Material thickness	Wall: 0.3 m Roof: 0.3 m	–
A/C Type	Canyon	
Occupancy and Energy Use	Residential Building Survey Data in Hong Kong	Mui (2006), Yu et al. (2019)

et al., 2003). Anthropogenic heat is not explicitly modeled in the standard ENVI-met configuration but can be included via user-defined sources (ENVI-met, 2025a). Additionally, ENVI-met includes detailed models for the prognostic surface energy balance equation to compute heat exchanges, soil heat and moisture fluxes, vegetation transpiration, shading, interception, building heat conduction, and momentum interactions within the urban canopy layer (ENVI-met, 2025a, 2025b). These components allow ENVI-met to capture complex interactions within the urban canopy layer, providing insights crucial for assessing the impact of urban design on local climate conditions (ENVI-met, 2025a). Fig. 4 illustrates the 3D representations of the ENVI-met model domains for the study sites.

2.4. SLUCM setup

SLUCM models urban neighborhoods as idealized street canyons with buildings of equal height on both sides to simulate urban surface-atmosphere interactions, suitable for mesoscale atmospheric models (Chen et al., 2021; Chen et al., 2024b; Kusaka et al., 2001). The model is coupled with a building energy model (BEM) to account for anthropogenic heat from air conditioning and occupancy, enhancing the simulation of heat dynamics in urban canyons (Chen et al., 2021; Chen et al., 2024b). The SLUCM solves canyon-mean heat and moisture balances for the atmospheric layer within the street canyon (see Fig. 4b). The radiative transfer scheme calculates net radiation for each surface facet (roof, wall, and road) by facet-mean view factors to account for shadowing and radiation reflection within urban canyons (Kusaka et al., 2001; Chen et al., 2021; Chen et al., 2024b). Unlike ENVI-met, which solves the surface energy balance prognostically for each grid cell, SLUCM uses a simplified approach that parameterizes heat fluxes at each surface based on mean properties and canyon geometry (Kusaka et al., 2001). Heat conduction process is solved using 1-D homogenous heat diffusion equation, while turbulent heat fluxes are parameterized using a bulk aerodynamic resistance method based on mean surface temperature and mean canyon air temperature (Kusaka et al., 2001). A logarithmic wind profile is applied above the urban canopy and an exponential wind profile is assumed within the canyon. Urban morphological parameters, such as building height and canyon width are derived from the Hong Kong Planning Department's Common Spatial Data Infrastructure Portal, applied as averages to represent the site's configurations (Chen et al., 2021b; Chen et al., 2024b). These parameters define the canyon geometry and surface properties in the SLUCM simulations.

Given that SLUCM simulations only output the average canyon T_a, and observational data were measured at a height of 1.5 m, modifications based on MOST were applied to evaluate SLUCM against these measurements (Fig. 5a). This approach follows previous studies (e.g., Pelliccioni et al., 2012) to estimate 1.5-m near-surface air temperature ($T_{1.5}$) and RH ($RH_{1.5}$). The potential temperature at a given height ($\theta(z)$) is calculated by adjusting the T_a of the first layer of the atmosphere (3 times the average building height) using the urban sensible heat flux (H):

$$\theta(z) = T_a + \left(\frac{H \times r_{ah}(z)}{r_a \times C_p}\right), \tag{6}$$

where $r_{ah}(z)$ is the aerodynamic resistance to sensible heat transfer at the height z, r_a is the aerodynamic resistance to momentum transfer between the surface and the first atmospheric layer and C_p is the specific heat capacity of air at constant pressure.

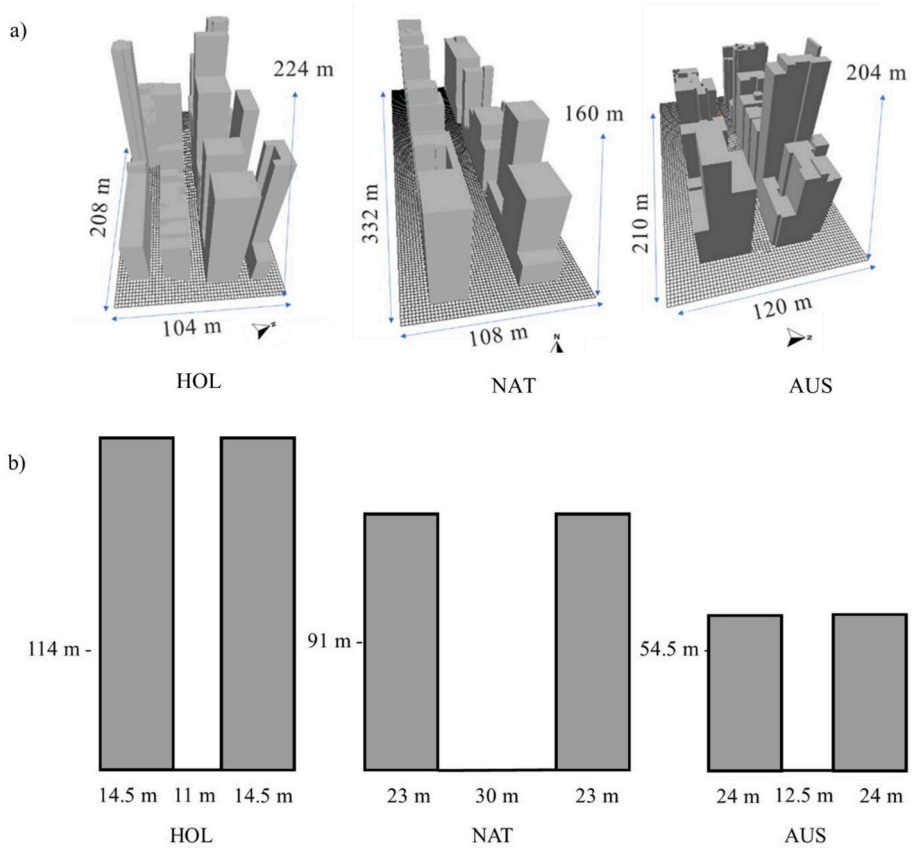

Fig. 4. Schematic representation of the 3D ENVI-met model domains (a) and 2D SLUCM models (b) for the three study sites.

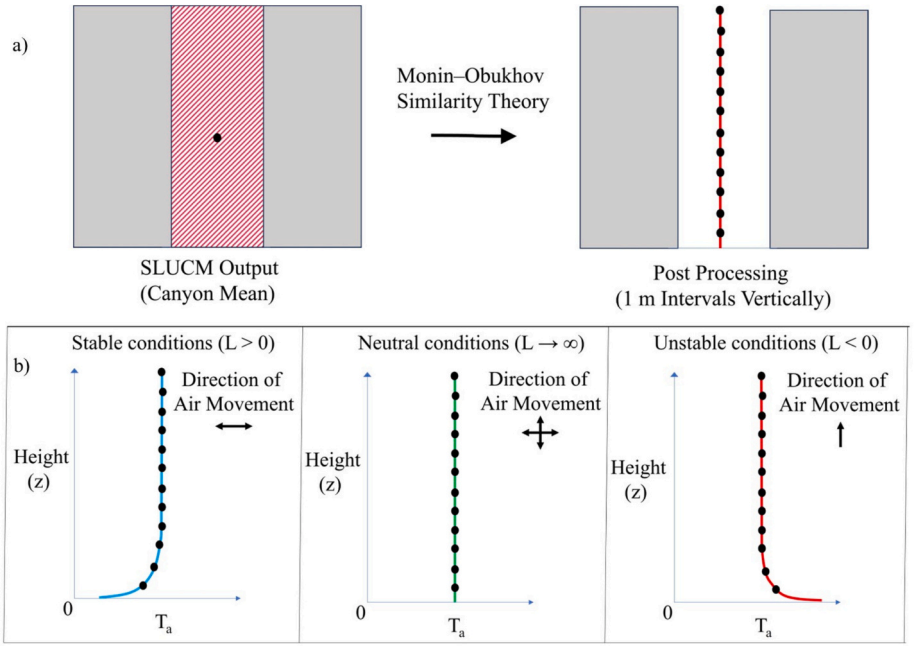

Fig. 5. Methodology for generating urban canyon vertical T_a profiles and classification of atmospheric stability regimes. (a) SLUCM canyon-mean output is post-processed using Monin–Obukhov Similarity Theory to derive vertical T_a profiles at 1 m intervals. (b) Characteristic T_a profiles with height (z) under stable (L > 0), neutral (L → ∞), and unstable (L < 0) conditions. Arrows denote typical vertical air movement associated with each stability regime.

Both $r_{ah}(z)$ and r_a are influenced by wind speed and surface roughness, but r_{ah} includes additional corrections for atmospheric stability that specifically affect heat transfer (Eqn. 7). These corrections that modify the resistance are based on stable, unstable, and neutral conditions, thus affecting the calculated T_a profile (Fig. 5b).

$$r_{ah}(z) = \frac{1}{k \times u_*}\left(\ln\left(\frac{Z_a}{z}\right) - Z_a L_{set} + z L_{set}\right) \tag{7}$$

where Z_a is the reference height (3 times the building height), k is the von Kármán constant, and u_* is the friction velocity. $Z_a L_{set}$ and $z L_{set}$ are stability correction terms based on MOST.

Similarly, the specific humidity at a given height $q(z)$ is calculated by adjusting the atmospheric specific humidity (q_a) using the latent heat flux (LE):

$$q(z) = q_a + \left(\frac{LE \times r_{ah}(z)}{r_a \times L_v}\right) \tag{8}$$

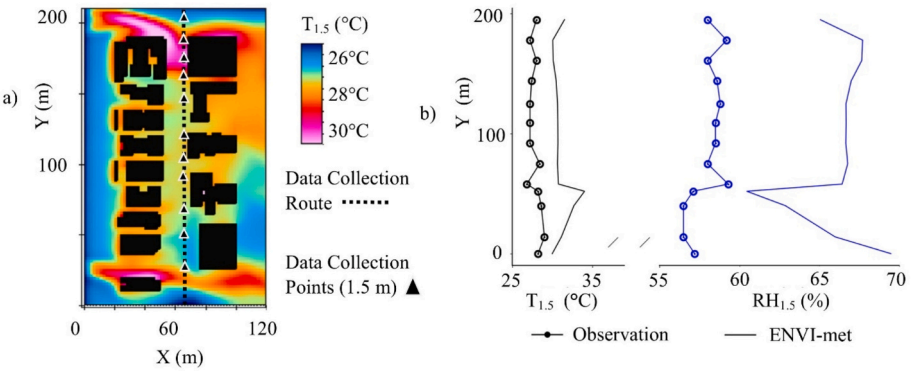

Fig. 6. Example of ENVI-met model validation at the AUS site on October 17, 2021, at 14:00. (a) Simulated $T_{1.5}$ (°C) distribution overlaid with the data collection route (b) Comparative analysis of the observed values and modeled $T_{1.5}$ (°C) and $RH_{1.5}$ (%).

where L_v is the latent heat of vaporization. The sensible heat flux (H) and latent heat flux (LE) used in Eqs. (6) and (8) represent the total values from the canyon, including anthropogenic releases. We set z = 1.5 m and obtained $T_{1.5}$ and $RH_{1.5}$ from the above calculations.

3. Results

3.1. Model validation

The validation process for ENVI-met involved a direct comparison between simulated and observational data at a pedestrian-level height of 1.5 m. Fig. 6a illustrates data collection points overlaid on ENVI-met's spatial simulation. To quantify model performance, the mean absolute error (MAE) was calculated for each pair of observed and simulated data points. The average MAE across all data points was then computed for each time period. Validation was performed separately 10:00, 14:00, and 19:00 to capture variations throughout the day. Fig. 6b shows an example illustration of this comparison at the AUS site in October at 14:00, where simulated data is compared against observational data along the data collection route.

The validation of SLUCM followed a similar principle to ENVI-met's validation but was adapted to its distinct modeling approach. Following the implementation of the SLUCM model output, detailed in section 2.4, the resulting output generated a vertical profile where each point represented an average value for the horizontal cross-section of the urban canyon at that height. Fig. 7a illustrates this validation methodology, with the data collection route overlaid with the horizontal axis average SLUCM output at 1.5 m. The MAE was then calculated for 10:00, 14:00, and 19:00. Fig. 7b presents a comparative example for the AUS site in October, showcasing the observations against SLUCM simulation $T_{1.5}$ and $RH_{1.5}$.

The evaluation results in Table 2 demonstrate that simulated $T_{1.5}$ generally has MAEs lower than 5 °C for both ENVI-met and SLUCM simulations, with one exception: the SLUCM simulation at the NAT site at 14:00 in September, which showed an MAE of 5.02 °C. ENVI-met simulations showed MAEs ranging from 0.17 °C to 4.94 °C, while SLUCM simulations varied between 0.10 °C and 5.02 °C. In terms of the overall mean MAE, ENVI-met simulations exhibited a lower value for $T_{1.5}$ simulations (1.39 °C) compared to SLUCM (1.5 °C), indicating slightly higher accuracy for ENVI-met (Table 2). These mean MAE results are comparable to previous evaluation studies in Asia. In Shenzhen, Wang et al. (2019) reported pedestrian-level T_a MAEs of 0.26 °C to 1.26 °C using ENVI-met, and Sun et al. (2021) found MAEs between 0.74 °C and 1.20 °C with SLUCM in a range southern coastal Chinese cities such as Shenzhen. Similar studies in Singapore showed comparable results, with Li et al. (2013) using SLUCM to find pedestrian-level T_a Mean Bias Errors of 0.11 °C to 1.04 °C, while Roth and Lim (2017) used ENVI-met and found MAEs of 0.4 °C to 1.21 °C.

It is noteworthy that the largest errors tended to occur during afternoon periods, suggesting a correlation between simulation accuracy with solar intensity. ENVI-met and SLUCM tend to have larger MAEs in the morning than in the evening (Average ENVI-met MAE: 1.7 °C in the morning, 0.12 °C in the evening; Mean SLUCM MAE: 1.01 °C in the morning, 0.54 °C in the evening). We suspect the overestimated T_a by both models in afternoon is caused by two reasons. First, model validation is conducted for the spatial mean of $T_{1.5}$ inside the canyon, while mobile measurements only measure one side of the canyon (potentially in shaded areas). Second, though ENVI-met and SLUCM have been previously tested over under various conditions, there are limited studies over neighborhoods with very high aspect ratios (mean building height/street width varies from 2.3 (AUS) to 7.9 (HOL) in this study). The errors here highlight the challenges both models face in accurately simulating pedestrian-level microclimate during periods of high solar radiation in high-rise neighborhoods, which shall be furthered examined in future studies.

$RH_{1.5}$ simulations exhibited larger errors compared to $T_{1.5}$ simulations, with MAEs ranging from 5.35 % to 20.49 % for ENVI-met and MAEs between 1.4 % and 16.49 % for SLUCM (Table 2). The AUS site consistently showed higher errors than other sites for both models, with ENVI-met and SLUCM recording average MAEs of 15.81 % and 8.35 %, respectively. Interestingly, while this site had the largest error in $RH_{1.5}$ simulations, it demonstrated the lowest error in $T_{1.5}$ simulations for both models. These findings align with previous studies that have documented larger ranges and lower reliability in pedestrian-level RH predictions compared to T_a for both models. For ENVI-met, Al-Hafith et al. (2019) reported MAEs of 12.81 % - 14.43 % in Cairo, Egypt. For SLUCM, Bilang et al. (2022)

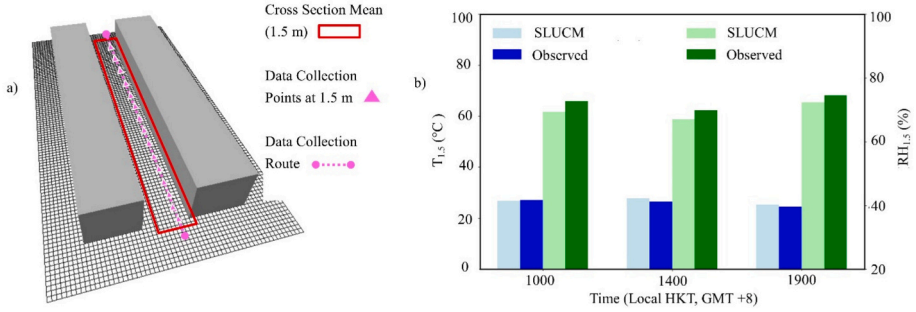

Fig. 7. Example of the SLUCM model validation through cross-canyon mean $T_{1.5}$ and $RH_{1.5}$. (a) Schematic representation of a simplified urban canyon utilized in SLUCM simulations with the cross-canyon output at a height of 1.5 m (b) Bar graphs comparing the simulated and observed mean $T_{1.5}$ (°C) and $RH_{1.5}$(%) at the AUS site on October 17th, 2021.

Table 2
Summary of MAEs for simulated $T_{1.5}$ (°C) and $RH_{1.5}$ (%) in parentheses from ENVI-met and SLUCM simulations.

Location	Time	Sep		Oct		Mean	
		ENVI-met	SLUCM	ENVI-met	SLUCM	ENVI-met	SLUCM
NAT	10:00	1.07 °C (16.37 %)	0.56 °C (11.56 %)	0.98 °C (14.42 %)	0.90 °C (3.73 %)	1.60 °C (13.1 %)	1.53 °C (7.03 %)
	14:00	4.94 °C (5.35 %)	5.02 °C (1.57 %)	2.02 °C (7.03 %)	1.18 °C (3.15 %)		
	19:00	0.42 °C (17.17 %)	0.47 °C (13.13 %)	0.19 °C (18.26 %)	0.10 °C (9.06 %)		
HOL	10:00	2.33 °C (20.16 %)	3.06 °C (12.35 %)	3.40 °C (17.67 %)	0.63 °C (9.15 %)	1.4 °C (15.07 %)	1.79 °C (7.3 %)
	14:00	0.43 °C (17.15 %)	4.9 °C (10.54 %)	0.65 °C (10.29 %)	1.11 °C (4.93 %)		
	19:00	0.17 °C (12.36 %)	0.28°C (1.4 %)	1.45 °C (12.82 %)	0.80 °C (5.46 %)		
AUS	10:00	1.00 °C (18.2 %)	0.56 °C (13.94 %)	1.46 °C (18.3 %)	0.38 °C (7.8 %)	1.17 °C (15.81 %)	1.34 °C (8.35 %)
	14:00	2.28 °C (13.25 %)	3.57 °C (4.54 %)	1.59 °C (8.08 %)	1.91 °C (1.83 %)		
	19:00	0.27 °C (20.49 %)	0.25 °C (16.49 %)	0.45 °C (16.57 %)	1.37 °C (5.51 %)		
Mean		1.43 °C (15.61 %)	2.07 °C (9.5 %)	1.35 °C (13.71 %)	0.93 °C (5.62 %)	1.39 °C (14.66 %)	1.5 °C (7.56 %)

reported MAEs of 7.22 % to 14 % in Metro Manila. Note that model validation mainly focuses on T_a for both ENVI-met and SLUCM, while errors on RH simulation has been rarely reported.

One major source of RH simulation error in this study could be sea breeze, whose impact on moisture transport may not be fully reflected in the meteorological forcing that drives the simulations. Acero and Arrizabalaga (2018) and Tsoka et al. (2018) also demonstrated that ENVI-met simulations have large RH errors in costal cities and suggested sea breeze play a major role in causing the error. Similarly, Tsiringakis et al. (2019) highlighted SLUCM's limitations in capturing sea breeze events, attributing this to both the temporal resolution of prescribed meteorological forcing and the model's inability to consider horizontal advection. These limitations are shared by both models, resulting in overestimation of $RH_{1.5}$. Their effects are exemplified by the AUS site at the tip of the Kowloon Peninsula in Tsim Sha Tsui, which exhibited the highest $RH_{1.5}$ errors among all sites. Despite efforts to select a site with a buffer from Victoria Harbour, sea breeze influences were likely captured in measurements but inadequately represented in simulations. However, ENVI-met's explicit modeling of turbulent mixing appears to compound these errors by overestimating moisture transport throughout the canyon, while SLUCM's parameterization scheme produces conservative and ultimately more accurate RH predictions. Nevertheless, our error ranges remain consistent with previously published validation studies, confirming both models fall within acceptable accuracy margins for urban microclimate modeling.

3.2. Diurnal cycle of microclimate

After evaluating the ENVI-met and SLUCM simulations for $T_{1.5}$ and $RH_{1.5}$, we expanded our investigation to examine the differences in diurnal patterns of T_2 and RH_2. While initial evaluations utilized observational data at 1.5 m due to availability constraints, subsequent analyses were conducted at 2 m above ground level. This adjustment aligns with widely accepted meteorological standards and enhances comparability with broader urban climate studies. For example, Wahba et al. (2019) validated the ENVI-met model at 1.5 m in arid climates and conducted analysis at a 2 m height. Russo et al. (2016) quantified the effect of urban treed streetscapes in Italy using ENVI-met simulations at a 2 m height. Li et al. (2013) employed SLUCM to investigate Singapore's tropical urban environment at a 2 m height. In addition to pedestrian level simulations, we calculated mean canyon air temperature (T_{can}) and relative humidity (RH_{can}). In this case, we directly used the output from SLUCM simulations and take the spatial mean from ENVI-met simulations. These canyon average simulations provide a multidimensional perspective on model performance, incorporating both vertical and horizontal aspects of the canyon environment.

Figs. 8 and 9 illustrate the diurnal cycle of ENVI-met and SLUCM simulations. Fig. 8 presents the direct output values of simulated parameters across the diurnal cycle, while Fig. 9 displays the corresponding delta values, quantifying the inter-model differences. A comparison of September and October reveals that October simulations are cooler and less humid, with ENVI-met showing an average decrease of 7.88 °C in T_2 and 8.17 % in RH_2, while SLUCM indicates reductions of 7.92 °C and 7.25 %, respectively. Notably, at the HOL site (Fig. 8i), T_2 simulations from ENVI-met are lower than those from SLUCM for September, whereas at the NAT and AUS sites, ENVI-met values are higher; this discrepancy is also evident in RH_2 simulations (Fig. 8j). Additionally, during September, SLUCM consistently exhibits higher T_2 values across all three sites (Fig. 8a,e,i), while ENVI-met shows greater values in T_{can} (Fig. 8c,g,k).

The differences between ENVI-met and SLUCM simulations—calculated as ENVI-met minus SLUCM, with negative values indicating higher SLUCM values—ranged from 1.63 °C to −4.62 °C for T_2 (see Fig. 9a). In contrast, the range for T_{can} simulations was

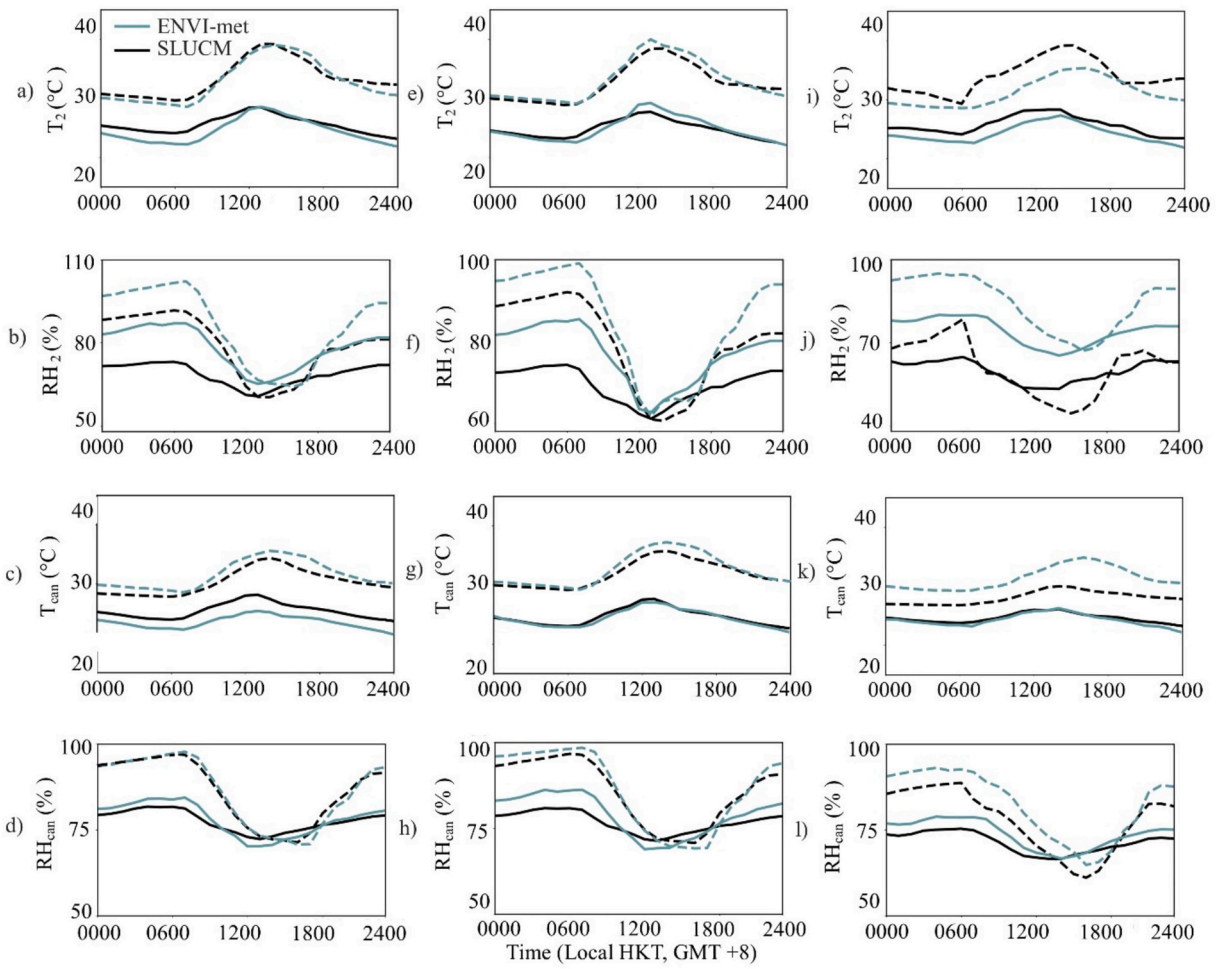

Fig. 8. Diurnal profiles of pedestrian-level T_2 (°C) and RH_2 (%), as well as T_{can} and RH_{can} at the AUS (first column), NAT (second column), and HOL (third column) sites simulated by the ENVI-met and SLUCM models. Within each panel, dashed lines represent September simulations and solid lines correspond to October simulations.

broader, spanning from 5.4 °C to −2.8 °C (Fig. 9c). For RH, the delta range for RH_{can} was between 7.9 % and − 4.3 % (Fig. 9d), which was smaller than the delta range for RH_2, which varied from 31.97 % to −1.58 % (Fig. 9b). Among the three study sites, the largest discrepancies between ENVI-met and SLUCM were observed at HOL for both 2 m and canyon mean simulations. Notably, ΔT_2 reached up to 4 °C and ΔRH_2 could be as high as 30 % in the September simulation. It is evident that these differences diminish after sunrise, suggesting that T_a increases are more sensitive to solar radiation in SLUCM.

The hourly delta values were averaged across the diurnal period to provide an overall comparison between the models, as outlined in Table 3. Averaged across September and October simulations, T_a differences in canyon-mean simulations exceeded those of 2 m simulations, while RH showed the opposite pattern. Specifically, T_{can} and RH_{can} differed by 0.48 °C and 1.75 % respectively, compared to −0.33 °C and 11.13 % at 2 m. The analysis reveals a mixed pattern in terms of which model predicts higher T_2, with three instances where ENVI-met shows higher values and three where SLUCM does. In terms of T_{can} prediction, SLUCM exhibited higher values in October, while ENVI-met yields higher values in all September simulations.

Table 4 summarizes the difference between pedestrian-level and canyon mean values. ENVI-met yielded T_{can} that was on average 0.55 °C cooler than T_2, while SLUCM showed an average 1.81 °C difference. It is noteworthy that the difference has a larger gap between September and October in SLUCM results, but not in ENVI-met results. In terms of RH, RH_{can} - RH_2 was <1 % for ENVI-met but was about 10 % for SLUCM. The observed reversal in the inter-model comparison, where SLUCM-simulated T_2 exceeded ENVI-met in September but was lower in October, while the opposite was true for the T_{can} simulations, can be attributed to SLUCM exhibiting a larger variation from T_{can} to T_2, particularly at the HOL site in September.

The HOL site, with its high aspect ratio (10.36:1) compared to sites with lower aspect ratios (AUS: 4.23:1, NAT: 3.03:1), has enhanced shading that limits solar radiation reaching the canyon floor. This thermal behavior aligns with Peng and Huang's (2022) findings that deep canyons in subtropical urban environments experience less thermal stress compared to those with lower aspect ratios. Notably, the HOL site exhibited unique model behavior, particularly evident in September when SLUCM showed T_{can} values

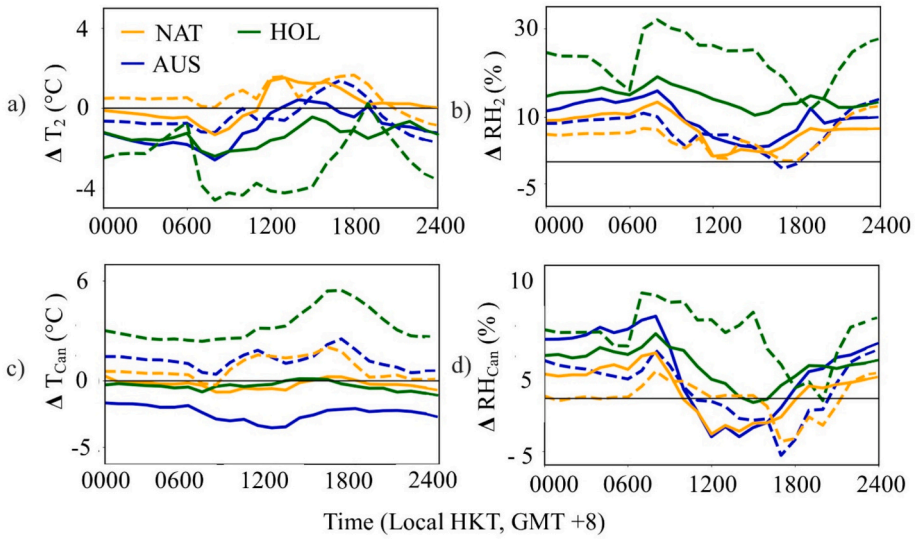

Fig. 9. Diurnal profiles of (a) ΔT_2, (b) ΔRH_2, (c) ΔT_{can}, and (d) RH_{can} between ENVI-met and SLUCM simulations. The dashed lines indicate September simulations, and solid lines represent October simulations. Positive values denote higher predictions by ENVI-met, while negative values signify higher predictions by SLUCM.

Table 3
Summary of mean ΔT_2, ΔRH_2, ΔT_{can}, and ΔRH_{can} between SLUCM and ENVI-met simulations.

Location	ΔT_2 (°C)		ΔRH_2 (%)		ΔT_{can} (°C)		ΔRH_{can} (%)	
	Sep	Oct	Sep	Oct	Sep	Oct	Sep	Oct
AUS	−0.41	−1.02	6.80	9.80	1.25	−1.93	0.66	2.13
HOL	−2.71	1.42	23.1	14.49	3.29	−0.30	4.75	2.44
NAT	0.62	0.12	5.12	7.46	0.75	−0.21	−0.05	0.58
Mean	−0.83	0.17	11.67	10.58	1.76	−0.81	1.79	1.72

Table 4
Averaged differences between canyon average and pedestrian-level simulations by SLUCM and ENVI-met.

Location	T_{can} - T_2 (°C)				RH_{can} - RH_2 (%)			
	ENVI-met		SLUCM		ENVI-met		SLUCM	
	Sep	Oct	Sep	Oct	Sep	Oct	Sep	Oct
AUS	−1.30	−0.97	−2.96	−0.10	0.60	0.69	6.74	8.22
HOL	−0.06	0.01	−5.93	−1.11	−1.54	−0.34	18.11	10.4
NAT	−0.55	−0.44	−0.67	−0.23	1.89	1.49	7.06	8.37
Mean	-0.64	-0.47	-3.19	-0.48	0.32	0.61	10.64	9.00

5.93 °C cooler than T_2 and RH_{can} 18.11 % higher compared to RH_2 (Table 4). These substantial variations likely stem from the site's narrow and deep geometry, which promotes more pronounced thermal stratification and turbulence suppression. Such conditions significantly affect the stability corrections in SLUCM's calculations, where reduced friction velocity (u*) in stable conditions diminishes turbulent production, leading to less effective heat and moisture transfer at lower heights. The impact of urban morphology is further complicated by the sites' meteorological forcing data. While NAT and AUS share data from the CoWIN Site at Po Leung Kuk Camões Tan Siu Lin Primary School due to their proximity on the Kowloon Peninsula, HOL relies on distinct meteorological data from St. Joseph's College on Hong Kong Island. As Salvati and Kolokotroni (2019) demonstrated, these differences in meteorological forcing can significantly impact microclimate modeling outcomes, potentially amplifying or masking geometry-induced effects.

These geometry-related findings highlight fundamental differences in how the models represent urban form and energy processes. ENVI-met's 3D approach provides detailed spatial resolution of radiative and convective processes within the canyon, but our results show this yields only marginal improvements in $T_{1.5}$ predictions in high-rise neighborhoods. However, the limitations of SLUCM's simplified 2D representation become more pronounced under high solar radiation conditions, particularly during afternoon periods when solar intensity peaks. As demonstrated by Hang et al. (2022), geometrical simplifications can significantly impact wind flows and urban energy processes. Comparison of September and October results further reveals the model differences, with ENVI-met showing a

tendency to overpredict T_a under high solar radiation conditions, particularly evident in September simulations where it predicted T_{can} 1.76 °C higher than SLUCM. Conversely, SLUCM, despite its spatial resolution limitations, produces more conservative T_a predictions during periods of higher solar radiation. For RH, ENVI-met consistently predicted higher RH_2 and RH_{can} values across all sites, with only one exception at the NAT site in September.

3.3. Vertical profiles of T_a and RH

To extend our analysis of model behavior, we examined the vertical profiles of T_a and RH. Generally, the profiles exhibit consistent patterns: T_a is elevated and RH is reduced at the ground surface and around buildings, as illustrated by a sample of the ENVI-met profiles at the NAT site in Sept at 10:00, 14:00, and 19:00 in Fig. 10. This phenomenon occurs because urban materials, such as concrete and asphalt, absorb and retain heat from solar radiation during the day. These materials possess high thermal mass, allowing them to store heat and release it slowly, which leads to higher near-surface T_a throughout the diurnal cycle (Shahmohamadi et al., 2011).

In our comparison of the two models, we observed consistently higher T_a predictions in ENVI-met simulations throughout the diurnal cycle, while RH predictions revealed more variability. This trend is illustrated in Fig. 11, which shows the vertical profiles of T_a and RH simulations from both ENVI-met and SLUCM for September and October at selected times. We calculated model differences using previously described methods—where negative values indicate that SLUCM predictions are greater. For instance, at the NAT site in September at 10:00, the mean difference between ENVI-met and SLUCM simulations was 1.05°C for T_a (Fig. 11a) and 0.84% for RH (Fig. 11c), while at 19:00, it was 1.49°C for T_a (Fig. 11b) and 0.61% for RH (Fig. 11d). In October, the discrepancies at 10:00 increased to 1.51°C for T_a (Fig. 11e) and -0.02% for RH (Fig. 11g), while at 19:00, they were 0.72°C for T_a (Fig. 11f) and 10.94% for RH (Fig. 11h). Across the diurnal cycle, average discrepancies between ENVI-met and SLUCM were notably larger in September than in October, with ranges of −7.44 °C to 5.32 °C (−14.19 % to 35 %) in September simulations, compared to −4.02 °C to 4.97 °C (−12.82 % to 21.96 %) in October simulations. Additionally, we found that the T_a difference was smaller during the daytime (1.05 °C) than at night (1.19 °C) in September simulations, whereas the opposite trend was observed in October (Daytime: 1.35 °C, Nighttime: 1.10 °C); here, the T_a difference was larger during the day but smaller at night. Conversely, RH exhibited opposite trends: larger differences were seen at night in September (Daytime: 2.52 %, Nighttime: 1.97 %) and during the day in October (Daytime: 1.1 %, Nighttime: 2.66 %). Overall, the vertical profile differences were larger for T_a but smaller for RH compared to the 2 m differences (Table 3). Temporally, the most significant average T_a differences occurred in the afternoon and evening (between 14:00 and 19:00) for both months, while the smallest differences were noted in the morning (between 7:00 and 10:00). For RH, the largest discrepancies consistently appeared in the morning hours (between 7:00 and 8:00), with the smallest differences occurring in the evening (between 14:00 and 20:00).

The models generally intersected at varying heights, with some exceptions. For instance, the models did not intersect in their T_a simulations for NAT in September at 19:00 (Fig. 11b). In the RH simulations, the HOL model did not consistently intersect, as seen in HOL September at 10:00 (Fig. 11c) and HOL October at 19:00 (Fig. 11g). The most substantial T_a differences across the diurnal period were found at higher elevations, averaging 81 m across sites in both September and October, with the smallest discrepancies observed at 1 m. In contrast, RH exhibited an inverse pattern, with the largest differences recorded at 1 m and the smallest at 67 m in September and 81 m in October. Largely, intersections in T_a simulations occurred at higher elevations during the September simulations compared to October. For example, at 10:00 in the HOL September T_a simulation (Fig. 11a), the intersection height was 22 m, while in October it dropped to 11 m (Fig. 11e). For RH, the intersection heights tended to be higher in October, as seen AUS at 19:00 where the

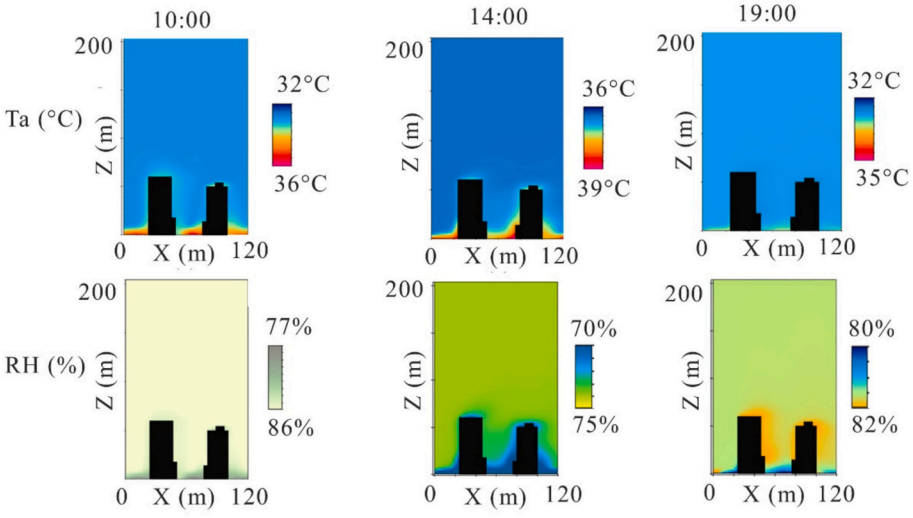

Fig. 10. ENVI-met vertical profile simulations at the NAT site for September, displaying morning at 10:00 (left column), afternoon at 14:00 (middle column), and evening at 19:00 (right column). The upper panels depict T_{at} (°C) and the lower panels show RH (%).

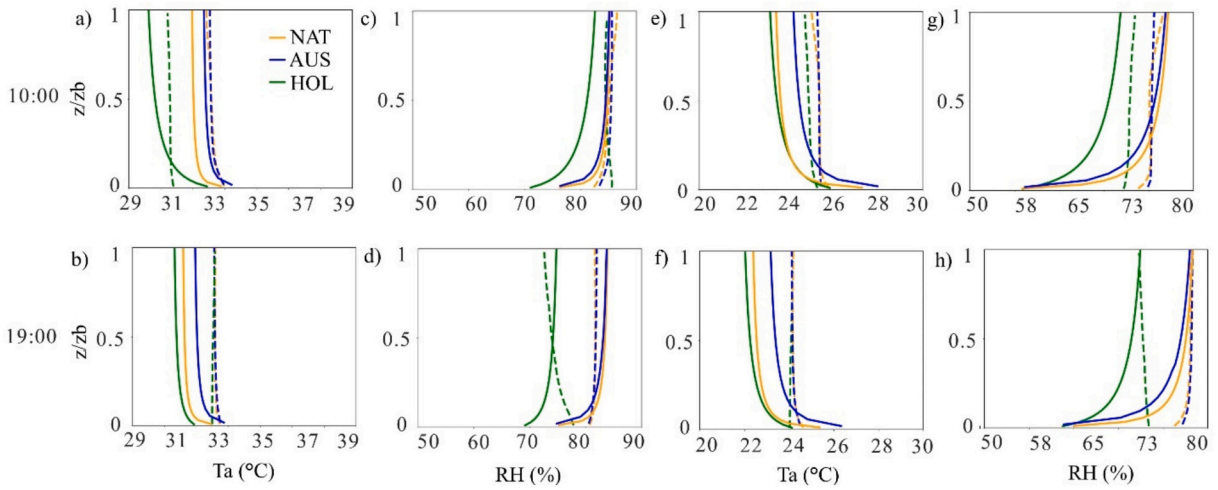

Fig. 11. Vertical profiles of T_a (°C) and RH (%) for the AUS (blue lines), NAT (orange lines), and HOL (green lines) sites at 10:00 (row 1) and 19:00 (row 2), as simulated by the ENVI-met and SLUCM models. The first column represents T_a simulations in September, the second column represents RH simulations in September, the third column represents T_a simulations in October, and the fourth column represents RH simulations in October. Within each panel, dashed lines represent ENVI-met simulations, while solid lines correspond to SLUCM simulations. (For interpretation of the references to colour in this figure legend, the reader is referred to the web version of this article.)

intersection was at 25 m in September (Fig. 11d) and 50 m in October (Fig. 11h).

When considering the differences between sites, both AUS and NAT deviated from the HOL site. The AUS site often showed an overall larger difference from HOL, but NAT tended to have the largest discrepancies. For example, in SLUCM simulations, the maximum T_a difference between NAT and HOL at the selected times (10:00, 14:00, 19:00) was 3.33 °C at a height of 1 m at 10:00 AM in September (Fig. 11a), which decreased to 1.38 °C in October (Fig. 11e). This pattern was mirrored in ENVI-met, where the largest T_a difference between NAT and HOL also occurred at 10:00 AM in September (3.31 °C at 91 m, Fig. 11a). In contrast, the AUS and NAT sites showed closer T_a differences, particularly in October, where the maximum difference was 0.69 °C at 1 m in SLUCM simulations and 0.22 °C at 1 m in ENVI-met simulations at 10:00 AM (Fig. 11e). ENVI-met's RH differences followed a similar seasonal trend; ENVI-met recorded a maximum RH difference between NAT and HOL of 2.81 % at 1 m in September at 10:00 (Fig. 11c), which diminished to 0.63 % in October at 19:00 at 1 m (Fig. 11h). In SLUCM, the largest RH discrepancies were observed between NAT and HOL in the morning at in September at 10:00 with a difference of 26.75 % (Fig. 11c) and in October simulations it was 11.33 % at 1 m at 19:00 (Fig. 11h).

Another notable pattern in the profiles is that ENVI-met simulations exhibited smaller gradients than SLUCM. This variability was assessed by evaluating the average change per m from 1 m to the building height (HOL: 107 m, NAT: 91 m AUS: 55 m) across the three sites. During daytime hours, ENVI-met demonstrated increasing T_a profiles from ground level, with average increases of 0.012 °C/m in September and 0.008 °C/m in October. In contrast, SLUCM revealed significant decreases in T_a with elevation, recording −0.052 °C/m in both September and October. For daytime RH, ENVI-met showed a change of −0.031 %/m in September and − 0.028 %/m in October, while SLUCM exhibited changes of 0.204 %/m in September and 0.213 %/m in October. At night, ENVI-met's total T_a change was −0.001 °C/m in September and − 0.002 °C/m in October; SLUCM recorded −0.036 °C/m in September and − 0.039 °C/m in October. For nighttime RH, ENVI-met indicated changes of 0.016 %/m in September and 0.013 %/m in October, whereas SLUCM showed 0.183 %/m in September and 0.177 %/m in October.

To place these differences into context, it is essential to consider the fundamental differences in model physics and their implications for the results of urban climate simulations. As discussed in the introduction, ENVI-met is a CFD model that utilizes a full three-dimensional approach with turbulence closure schemes, solving the flow field for each grid cell and time step. This capability allows ENVI-met to capture the interactions between airflow, buildings, and ground surfaces within urban canyons, as well as the effects of surrounding urban context in the model domain. In contrast, the applied MOST to the SLUCM incorporates limited vertical mixing through stability corrections. While the MOST serves as a first-order approximation for vertical turbulent mixing, it inadequately resolves the complexities of horizontal and non-homogeneous flow (Optis et al., 2016). Consequently, SLUCM's representation of turbulence is limited. As demonstrated in the T_a and RH vertical profiles (Fig. 10), as well as the small T_{can}-T_2 and RH_{can}-RH_2 differences of ENVI-met simulations (Table 3), increased turbulence mixing results in a more homogeneous distribution of T_a and RH in ENVI-met results. This turbulent transport not only elevates T_a but also facilitates moisture transport, resulting in higher RH values. These profiles reflect more realistic conditions, particularly in LCZ 1 sites that have large aspect ratios. This behavior was documented by Govehovitch et al. (2021), who noted that deep canyons with high height-to-width (H/W) ratios often exhibit less variation in T_a with height due to reduced radiative cooling and increased solar radiation absorption.

These findings contribute to the ongoing discussion about turbulent mixing representations in atmospheric models. Li et al. (2021) demonstrated that in convective boundary layers, mass-flux transport and eddy-diffusivity are interconnected rather than

independent, suggesting that unified parameterization approaches could improve vertical transport predictions. This is particularly relevant to our findings regarding SLUCM's limitations, as it relies on MOST which assumes independent transport processes. The vertical profile discrepancies we observed between SLUCM and ENVI-met, particularly in T_a gradients (0.052 °C/m in SLUCM versus 0.012 °C/m in ENVI-met during daytime), are consistent with findings from Akinlabi et al. (2022), who demonstrated that dispersive fluxes and spatial heterogeneities in urban environments can significantly affect vertical transport processes, especially in areas with complex building morphologies.

In the end, it is worth pointing out that explicit representation of buildings in ENVI-met leads to a large computational cost. In terms of the computational demand, ENVI-met requires significantly more resources - a 24-h simulation with a 200 m × 200 m model domain typically takes 1–3 days to complete, whereas SLUCM can finish the simulation for the same domain within 5 min. The high computational demand of ENVI-met has also been reported in previous studies (Forouzandeh (2021). For example, Salvati and Kolokotroni (2019) found that a 48-h ENVI-met simulation required 38 h of processing time on a supercomputer. This trade-off between computational efficiency and simulation resolution needs to be considered when one selects models for microclimate simulation.

4. Conclusion and recommendations

This research undertook a detailed comparative analysis of urban climate simulations using the SLUCM and ENVI-met models, set against the backdrop of three compact high-rise street canyons in Hong Kong. Results show that both the SLUCM and ENVI-met models have reliable capabilities in simulating pedestrian-level T_a, with ENVI-met showing slightly higher accuracy. However, SLUCM distinctly outperformed ENVI-met in predicting pedestrian-level RH. In terms of the differences between ENVI-met and SLUCM simulations across the diurnal cycle, SLUCM simulations had higher predictions closer to the ground (T_2), while ENVI-met showed higher T_a predictions when considering the canyon mean (T_{can}, Vertical T_a). RH was consistently higher in all ENVI-met simulations (RH_2, R_{can}, Vertical RH). The HOL site, characterized by the highest aspect ratio, consistently demonstrated cooler T_a and lower RH throughout the day, attributed to enhanced shading that limits solar radiation exposure and potential wind tunneling effects that promote cooling. This trend aligns with previous findings indicating that deeper canyons in subtropical urban environments experience reduced thermal stress compared to those with lower aspect ratios.

Model performance variations of T_2 were primarily driven by solar radiation, with significant differences in September and October. To extrapolate SLUCM outputs vertically, MOST was applied with the result of steep T_a and RH gradients, while ENVI-met's explicit turbulence modeling yielded more homogeneous profiles. ENVI-met's 3D approach excels in resolving detailed flow fields and radiation patterns but produces warmer, more humid, and homogeneous microclimates at high computational cost. SLUCM offers computational efficiency with robust anthropogenic heat considerations despite its simplified 2D representation. Research focus should guide model selections: ENVI-met suits for heterogeneous neighborhoods where morphology plays important roles in determining the vertical mixing. In coastal regions, nevertheless, ENVI-met shall be used with caution as overestimated RH can lead to overestimation in outdoor thermal stress. For SLUCM, its simulated T_2 and T_{can} agree reasonably well with the ENVI-met model. However, the simulated vertical gradient is too large within the canopy layer that it tends to substantially overestimate T_a at a height less than 1 m.

Based on these findings, we propose three key recommendations for improving both models' capabilities. First, we recommend enhancing SLUCM's turbulence parameterization. The primary approach involves implementing an advanced Eddy-Diffusivity Mass Transfer Approach that would better represent vertical mixing processes in urban environments. As demonstrated by Li et al. (2021), this approach would utilize eddy diffusivity coefficients that depend on turbulent kinetic energy (TKE) and mixing length to more accurately quantify the efficiency of turbulent eddies in mixing scalar quantities like T_a and RH. Building on Lu et al.'s (2024) recent advances, this implementation would require reformulating SLUCM's aerodynamic resistance equations to incorporate separate diffusion coefficients for momentum and TKE, along with a mass-flux term. These modifications should be complemented by a Dispersive Flux Parameterization scheme and improved drag coefficient integration to better represent surface roughness effects on airflow.

Second, given the limitations of both models in capturing RH in Hong Kong, we recommend a coupling with mesoscale models for better representation of sea breeze impacts on urban microclimate. Simulation accuracy of SLUCM and ENVI-met depends on the meteorological forcing, which is usually obtained from nearby weather stations. However, for coastal regions, forcing at one specific location may not capture the moisture advection by sea breeze due to the complex wind flow in urban environments. Extending the ENVI-met domain to cover water areas will significantly increase the computational demand and thus is not feasible. WRF-CFD coupling methods, as demonstrated by He et al. (2024), can effectively capture the penetration of sea/land breeze with various distances from the coastline. The WRF model can efficiently simulate regional land/sea breeze with reasonable computational costs, and the output meteorological forcing that contains the impact of land/sea breeze can be utilized to drive ENVI-met/SLUCM simulations. In this way, accurate urban microclimate simulation in coastal urban environments can be achieved with a reasonable computational cost. Such an approaches will be particularly valuable for lake/coastal sites where lake/sea breeze dynamics significantly influence local microclimate conditions.

The primary limitation of this study arises from the temporal and vertical resolution of the observational data, with data collection restricted to three daily intervals—morning, afternoon, and evening—limiting the analysis to specific time points rather than continuous diurnal trends. Additionally, the evaluation of $T_{1.5}$ and $RH_{1.5}$ was constrained to pedestrian-level, leaving the error along the vertical profiles' unknown. To address these limitations, future studies could focus on evaluating the models against full diurnal and vertically resolved profiles to provide a more comprehensive assessment of their performance. Furthermore, future research could

expand the assessment of these models across diverse terrains, incorporating various LCZ types and vegetative covers. This approach will enable a more comprehensive understanding of the models' behavior and help to fine-tune the error margins. Such studies will not only refine the predictive precision of urban climate models but will also enhance their practical applicability in urban planning and the development of strategies to mitigate climate change impacts in densely populated cities like Hong Kong.

CRediT authorship contribution statement

Jonathan Lieber: Writing – review & editing, Writing – original draft, Visualization, Methodology, Investigation, Formal analysis. **Xuan Chen:** Writing – review & editing, Methodology, Investigation. **Liutao Chen:** Writing – review & editing, Methodology, Investigation. **Jiachuan Yang:** Writing – review & editing, Supervision, Project administration, Methodology, Funding acquisition, Conceptualization.

Declaration of generative AI and AI-assisted technologies in the writing process

During the preparation of this work the author(s) used Poe in order to improve writing and grammar. After using this tool/service, the author(s) reviewed and edited the content as needed and take(s) full responsibility for the content of the publication.

Declaration of competing interest

The authors declare that they have no known competing financial interests or personal relationships that could have appeared to influence the work reported in this paper.

Acknowledgement

This work was supported by the National Natural Science Foundation of China for Excellent Young Scientists (42322903).

Data availability

Data will be made available on request.

References

Acero, J.A., Arrizabalaga, J., 2018. Evaluating the performance of ENVI-met model in diurnal cycles for different meteorological conditions. Theor. Appl. Climatol. 131 (1), 455–469. https://doi.org/10.1007/s00704-016-1971-y.

Afshari, A., Ramirez, N., 2021. Improving the accuracy of simplified urban canopy models for arid regions using site-specific prior information. Urban Clim. 35, 100722. https://doi.org/10.1016/j.uclim.2020.100722.

Akinlabi, E., Maronga, B., Giometto, M.G., Li, D., 2022. Boundary-layer meteorology dispersive fluxes within and over a real urban canopy: a large-eddy simulation study. Bound.-Layer Meteorol. https://doi.org/10.1007/s10546-022-00725-6.

Al-Hafith, O., Satish, B.K., De Wilde, P., 2019. Envi-MET validation and sensitivity analysis using field measurements in a hot arid climate: the impact of courtyard geometry on its mean radiant temperature. IOP Conf. Ser. Earth Environ. Sci. https://doi.org/10.1088/1755-1315/329/1/012040.

Berardi, U., Jandaghian, Z., Graham, J., 2020. Effects of greenery enhancements for the resilience to heat waves: a comparison of analysis performed through mesoscale (WRF) and microscale (ENVI-met) modeling. Sci. Total Environ. 747, 141300. https://doi.org/10.1016/J.SCITOTENV.2020.141300.

Bilang, R.G.J.P., Blanco, A.C., Santos, J.A.S., Olaguera, L.M.P., 2022. Simulation of urban Heat Island during a high-heat event using WRF urban canopy models: a case study for metro Manila. Atmosphere 13 (10). https://doi.org/10.3390/atmos13101658. Article 10.

Cao, Q., Huang, H., Hong, Y., Huang, X., Wang, S., Wang, L., Wang, L., 2022. Modeling intra-urban differences in thermal environments and heat stress based on local climate zones in Central Wuhan. Build. Environ. 225, 109625. https://doi.org/10.1016/j.buildenv.2022.109625.

Chatzinikolaou, E., Chalkias, C., Dimopoulou, E., 2018. Urban Microclimate Improvement Using Envi-Met Climate Model. https://doi.org/10.5194/isprs-archives-XLII-4-69-2018.

Chen, L., Zheng, X., Yang, J., Yoon, J.H., 2021. Impact of BIPV windows on building energy consumption in street canyons: model development and validation. Energ. Buildings 249, 111207. https://doi.org/10.1016/J.ENBUILD.2021.111207.

Chen, X., Wang, H., Yang, J., 2024a. Effect of green blue spaces on the urban thermal environment: a field study in Hong Kong. Urban Clim. 55, 101912. https://doi.org/10.1016/j.uclim.2024.101912.

Chen, L., Yang, J., Zheng, X., 2024b. Modelling the impact of building energy consumption on urban thermal environment: the bias of the inventory approach. Urban Clim. 53, 101802. https://doi.org/10.1016/J.UCLIM.2023.101802.

Community Weather Information Network, 2023. Historical Data Download (Hourly-Average). https://cowin.hku.hk/.

Conigliaro, E., Monti, P., Leuzzi, G., Cantelli, A., 2021. A three-dimensional urban canopy model for mesoscale atmospheric simulations and its comparison with a two-dimensional urban canopy model in an idealized case. Urban Clim. 37, 100831. https://doi.org/10.1016/j.uclim.2021.100831.

Cortes, A., Rejuso, A.J., Santos, J.A., Blanco, A., 2022. Evaluating mitigation strategies for urban heat island in Mandaue City using ENVI-met. J. Urban Manag. 11 (1), 97–106. https://doi.org/10.1016/J.JUM.2022.01.002.

Crank, P.J., Middel, A., Wagner, M., Hoots, D., Smith, M., Brazel, A., 2020. Validation of seasonal mean radiant temperature simulations in hot arid urban climates. Sci. Total Environ. 749, 141392. https://doi.org/10.1016/j.scitotenv.2020.141392.

CSDI, 2022. Hong Kong CSDI Portal. https://portal.csdi.gov.hk/csdi-webpage/.

Di Giuseppe, E., Ulpiani, G., Cancellieri, C., Di Perna, C., D'Orazio, M., Zinzi, M., 2021. Numerical modelling and experimental validation of the microclimatic impacts of water mist cooling in urban areas. Energ. Buildings 231, 110638. https://doi.org/10.1016/J.ENBUILD.2020.110638.

Eingrüber, N., Scherer, D., 2023. Investigation of the ENVI-met model sensitivity to different wind direction forcing data in a heterogeneous urban environment. Adv. Sci. Res. 20, 65–74. https://doi.org/10.5194/asr-20-65-2023.

ENVI-met, 2025a. Model Concept: Urban Microclimate Simulation Processes. https://envi-met.info/doku.php?id=intro:modelconcept.

ENVI-met, 2025b. ENVI-met. A Holistic Microclimate Modelling System. https://envi-met.info/doku.php?id=root:start.

ENVI-met, 2025c. [TURBULENCE] Section. https://envi-met.info/doku.php?id=turbulence.

Ernest Orlando Lawrence Berkeley National Laboratory, 2014. Weather Data Hourly Interpolation: Input Output Reference — EnergyPlus 8.0. https://bigladdersoftware.com/epx/docs/8-0/input-output-reference/page-098.html.
European Commission, 2018. Consequences of Climate Change - European Commission. https://climate.ec.europa.eu/climate-change/consequences-climate-change_en.
Forouzandeh, A., 2021. Prediction of surface temperature of building surrounding envelopes using holistic microclimate ENVI-met model. Sustain. Cities Soc. 70, 102878. https://doi.org/10.1016/j.scs.2021.102878.
Fu, Q., Zheng, Z., Sarker, M.N.I., Lv, Y., 2024. Combating urban heat: systematic review of urban resilience and adaptation strategies. Heliyon 10 (17), e37001. https://doi.org/10.1016/j.heliyon.2024.e37001.
Govehovitch, B., Thebault, M., Bouty, K., Giroux-Julien, S., Peyrol, É., Guillot, V., Ménézo, C., Desthieux, G., Mainini, A.G., Lobaccaro, G., Košir, M., Diego, J., Cadena, B., Balaras, C.A., Lyon, C.B., 2021. Numerical validation of the radiative model for the solar cadaster developed for greater Geneva. Appl. Sci. 11 (17), 7806. https://doi.org/10.3390/app11178086.
Government of Hong Kong, 2022. GovHK: Hong Kong – the Facts. https://www.gov.hk/en/about/abouthk/facts.htm.
He, J., Kang, Y., Wang, Y., Gu, Y., Zhong, K., 2024. Effects of sea-land breeze on air pollutant dispersion in street networks with different distances from coast using WRF-CFD coupling method. Sustain. Cities Soc. 115, 105757. https://doi.org/10.1016/j.scs.2024.105757.
Hidalgo, J., Masson, V., Baklanov, A., Pigeon, G., Gimeno, L., 2008. Advances in urban climate modeling. Ann. N. Y. Acad. Sci. 1146 (1), 354–374. https://doi.org/10.1196/ANNALS.1446.015.
Huttner, S., 2012. *Further development and application of the 3D microclimate simulation ENVI-met* [doctoral dissertation, Johannes Gutenberg-Universität Mainz]. Gutenberg Open Sci. https://doi.org/10.25358/openscience-2022.
Karlický, J., Huszár, P., Halenka, T., Belda, M., Žák, M., Pišoft, P., Mikšovský, J., 2018. Multi-model comparison of urban heat island modeling approaches. Atmos. Chem. Phys. 18, 10655–10674. https://doi.org/10.5194/acp-18-10655-2018.
Khan, A., Papazoglou, E.G., Cartalis, C., Philippopoulos, K., Vasilakopoulou, K., Santamouris, M., 2022. On the mitigation potential and urban climate impact of increased green infrastructures in a coastal Mediterranean city. Build. Environ. 221, 109264. https://doi.org/10.1016/J.BUILDENV.2022.109264.
Krayenhoff, E.S., Broadbent, A.M., Zhao, L., Georgescu, M., Middel, A., Voogt, J.A., Martilli, A., Sailor, D.J., Erell, E., 2021. Cooling hot cities: a systematic and critical review of the numerical modelling literature. Environ. Res. Lett. 16 (5), 053007. https://doi.org/10.1088/1748-9326/ABDCF1.
Kusaka, H., Kimura, F., 2004. Coupling a single-layer urban canopy model with a simple atmospheric model: impact on urban heat island simulation for an idealized case. J. Meteorol. Soc. Jpn. 82 (1), 67–80. https://doi.org/10.2151/jmsj.82.67.
Kusaka, H., Kondo, H., Kikegawa, Y., Kimura, F., 2001. A simple single-layer urban canopy model for atmospheric models: comparison with multi-layer and slab models. Bound.-Layer Meteorol. 101 (3), 329–358. https://doi.org/10.1023/A:1019207923078.
Laaidi, K., Zeghnoun, A., Dousset, B., Bretin, P., Vandentorren, S., Giraudet, E., Beaudeau, P., 2012. The impact of heat islands on mortality in Paris during the august 2003 heat wave. Environ. Health Perspect. 120 (2), 254–259. https://doi.org/10.1289/ehp.1103532.
Lam, Y.F., Ong, C.W., Wong, M.H., Sin, W.F., Lo, C.W., 2021. Improvement of community monitoring network data for urban heat island investigation in Hong Kong. Urban Clim. 37, 100852. https://doi.org/10.1016/J.UCLIM.2021.100852.
Lee, T.C., Chan, H.S., Ginn, E.W.L., Wong, M.C., 2011. Long-term trends in extreme temperatures in Hong Kong and southern China. Adv. Atmos. Sci. 28 (1), 147–157. https://doi.org/10.1007/S00376-010-9160-X.
Li, X.-X., Koh, T.-Y., Entekhabi, D., Roth, M., Panda, J., Norford, L.K., 2013. A multi-resolution ensemble study of a tropical urban environment and its interactions with the background regional atmosphere. J. Geophys. Res. Atmos. 118, 9804–9818. https://doi.org/10.1002/jgrd.50795.
Li, Z., Zhou, Y., Wan, B., Chung, H., Huang, B., Liu, B., 2019. Model evaluation of high-resolution urban climate simulations: using the WRF/Noah LSM/SLUCM model (version 3.7.1) as a case study. Geosci. Model Dev. 12 (11), 4571–4584. https://doi.org/10.5194/GMD-12-4571-2019.
Li, Q., Cheng, Y., Gentine, P., 2021. Connection between mass flux transport and eddy diffusivity in convective atmospheric boundary layers. Geophys. Res. Lett. 48 (8). https://doi.org/10.1029/2020GL092073 e2020GL092073.
Lipson, M.J., Grimmond, S., Best, M., Abramowitz, G., Coutts, A., Tapper, N., Baik, J.-J., Beyers, M., Blunn, L., Boussetta, S., Bou-Zeid, E., De Kauwe, M.G., de Munck, C., Demuzere, M., Fatichi, S., Fortuniak, K., Han, B.-S., Hendry, M.A., Kikegawa, Y., Pitman, A.J., 2024. Evaluation of 30 urban land surface models in the urban-PLUMBER project: phase 1 results. Q. J. R. Meteorol. Soc. 150 (758), 126–169. https://doi.org/10.1002/qj.4589.
Liu, Z., Cheng, W., Jim, C.Y., Morakinyo, T.E., Shi, Y., Ng, E., 2021. Heat mitigation benefits of urban green and blue infrastructures: a systematic review of modeling techniques, validation and scenario simulation in ENVI-met V4. Build. Environ. 200, 107939. https://doi.org/10.1016/J.BUILDENV.2021.107939.
Lu, J., Nazarian, N., Hart, M.A., Krayenhoff, E.S., Martilli, A., 2024. A one-dimensional urban flow model with an eddy-diffusivity mass-flux (EDMF) scheme and refined turbulent transport (MLUCM v3.0). Geosci. Model Dev. 17, 2525. https://doi.org/10.5194/gmd-17-2525-2024.
Masson, V., Heldens, W., Bocher, E., Bonhomme, M., Buchhold, R., Esch, T., 2020. City-descriptive input data for urban climate models: model requirements, data sources and challenges. Urban Clim. 31, 100536. https://doi.org/10.1016/j.uclim.2019.100536.
Morakinyo, T.E., Dahanayake, K.W.D., Kalani, C., Ng, E., Chow, C.L., 2017. Temperature and cooling demand reduction by green-roof types in different climates and urban densities: a co-simulation parametric study. Energ. Buildings 145, 226–237. https://doi.org/10.1016/j.enbuild.2017.03.066.
Morakinyo, T.E., Lau, K.K.-L., Ren, C., Ng, E., 2018. Performance of Hong Kong's common trees species for outdoor temperature regulation, thermal comfort and energy saving. Build. Environ. 137, 157–170. https://doi.org/10.1016/j.buildenv.2018.04.012.
Morakinyo, T.E., Ouyang, W., Lau, K.K.-L., Ren, C., Ng, E., 2020. Right tree, right place (urban canyon): tree species selection approach for optimum urban heat mitigation - development and evaluation. Sci. Total Environ. 719, 137461. https://doi.org/10.1016/j.scitotenv.2020.137461.
Mui, K.W., 2006. An Occupant Load Survey for Residential Buildings in Hong Kong. https://research.polyu.edu.hk/en/publications/an-occupant-load-survey-for-residential-buildings-in-hong-kong.
Oke, T.R., 1982. The energetic basis of the urban heat island. Q. J. R. Meteorol. Soc. 108 (455), 1–24. https://doi.org/10.1002/qj.49710845502.
Oke, T.R., Mills, G., Christen, A., Voogt, J.A., 2017. Concepts. In: Urban Climates, pp. 14–43. https://doi.org/10.1017/9781139016476.003.
Optis, M., Monahan, A., Bosveld, F.C., 2016. Limitations and breakdown of Monin-Obukhov similarity theory for wind profile extrapolation under stable stratification. Wind Energy 19 (6), 1053–1072. https://doi.org/10.1002/WE.1883.
Ozkeresteci, I., Crewe, K., Brazel, A.J., Bruse, M., 2003. Use and evaluation of the Envi-Met model for environmental design and planning: An experiment on linear parks. In: *Proceedings of the 21st International Cartographic Conference (ICC)*, Durban, South Africa, 10–16 August 2003. Cartographic Renaissance. The International Cartographic Association. In: https://icaci.org/files/documents/ICC_proceedings/ICC2003/Papers/516.pdf.
Pelliccioni, A., Monti, P., Gariazzo, C., Leuzzi, G., 2012. Some characteristics of the urban boundary layer above Rome, Italy, and applicability of Monin-Obukhov similarity. Environ. Fluid Mech. 12 (5), 405–428. https://doi.org/10.1007/S10652-012-9246-3.
Peng, M., Huang, H., 2022. The synergistic effect of urban canyon geometries and greenery on outdoor thermal comfort in humid subtropical climates. Front. Environ. Sci. 10. https://doi.org/10.3389/fenvs.2022.851810.
Ritchie, H., Samborska, V., Roser, M., 2018. Urbanization - Our World in Data. https://ourworldindata.org/urbanization.
Roth, M., Lim, V.H., 2017. Evaluation of canopy-layer air and mean radiant temperature simulations by a microclimate model over a tropical residential neighbourhood. Build. Environ. 112, 177–189. https://doi.org/10.1016/j.buildenv.2016.11.026.
Russo, A., Escobedo, F.J., Zerbe, S., Russo, A., Escobedo, F.J., Zerbe, S., 2016. Quantifying the local-scale ecosystem services provided by urban treed streetscapes in Bolzano, Italy. AIMS Environ. Sci. 3 (1), 58–76. https://doi.org/10.3934/ENVIRONSCI.2016.1.58.
Salata, F., Golasi, I., de Lieto Vollaro, R., de Lieto Vollaro, A., 2016. Urban microclimate and outdoor thermal comfort: a proper procedure to fit ENVI-met simulation outputs to experimental data. Sustain. Cities Soc. 26, 318–343. https://doi.org/10.1016/J.SCS.2016.07.005.
Salvati, A., Kolokotroni, M., 2019. Microclimate Data for Building Energy Modelling: Study on ENVI-Met Forcing Data. https://doi.org/10.26868/25222708.2019.210544.
Shahmohamadi, P., Che-Ani, A.I., Maulud, K.N.A., Tawil, N.M., Abdullah, N.A.G., 2011. The impact of anthropogenic heat on formation of urban heat island and energy consumption balance. Urban Stud. Res. https://doi.org/10.1155/2011/497524. Article 497524.

Shinzato, P., Simon, H., Duarte, D.H.S., Bruse, M., 2019. Calibration process and parametrization of tropical plants using ENVI-met V4: São Paulo case study. Archit. Sci. Rev. 62 (2), 112–125. https://doi.org/10.1080/00038628.2018.1563522.

Simon, H., Sinsel, T., Bruse, M., 2021. Advances in simulating radiative transfer in complex environments. Appl. Sci. (Switzerland) *11* (12). https://doi.org/10.3390/APP11125449. Article 5449.

Singh, N., Singh, S., Mall, R.K., 2020. Urban ecology and human health: implications of urban heat island, air pollution and climate change nexus. In: Urban Ecology: Emerging Patterns and Social-Ecological Systems, pp. 317–334. https://doi.org/10.1016/B978-0-12-820730-7.00017-3.

Stewart, I.D., Oke, T.R., 2012. Local climate zones for urban temperature studies. Bull. Am. Meteorol. Soc. 93 (12), 1879–1900. https://doi.org/10.1175/BAMS-D-11-00019.1.

Sun, Y., Zhang, N., Miao, S., Kong, F., Zhang, Y., Li, N., 2021. Urban morphological parameters of the Main cities in China and their application in the WRF model. J. Adv. Model. Earth Syst. 13 (8). https://doi.org/10.1029/2020MS002382 e2020MS002382.

Tsiringakis, A., Steeneveld, G.J., Holtslag, A.A.M., Kotthaus, S., Grimmond, S., 2019. On- and off-line evaluation of the single-layer urban canopy model in London summertime conditions. Q. J. R. Meteorol. Soc. 145 (721), 1474–1489. https://doi.org/10.1002/QJ.3505.

Tsoka, S., Tsikaloudaki, A., Theodosiou, T., 2018. Analyzing the ENVI-met microclimate model's performance and assessing cool materials and urban vegetation applications: a review. Sustain. Cities Soc. 43, 55–76. https://doi.org/10.1016/J.SCS.2018.08.009.

Wahba, S., Kamil, B., Nassar, K., Abdelsalam, A., 2019. Green envelop impact on reducing air temperature and enhancing outdoor thermal comfort in arid climates. Civil Engineer. J. 5 (5). https://doi.org/10.28991/cej-2019-03091317.

Wang, Y., Ni, Z., Chen, S., Xia, B., 2019. Microclimate regulation and energy saving potential from different urban green infrastructures in a subtropical city. J. Clean. Prod. 226, 913–927. https://doi.org/10.1016/j.jclepro.2019.04.114.

Yang, J., Wang, Z.-H., Kaloush, K.E., Dylla, H., 2016. Effect of pavement thermal properties on mitigating urban heat islands: a multi-scale modeling case study in Phoenix. Build. Environ. 108, 110–121. https://doi.org/10.1016/j.buildenv.2016.08.021.

Yu, C., Du, J., Pan, W., 2019. Improving accuracy in building energy simulation via evaluating occupant behaviors: a case study in Hong Kong. Energ. Buildings 202. https://doi.org/10.1016/j.enbuild.2019.109373. Article 109373.

Zhao, L., Oleson, K., Bou-Zeid, E., Krayenhoff, E.S., Bray, A., Zhu, Q., Zheng, Z., Chen, C., Oppenheimer, M., 2021. Global multi-model projections of local urban climates. Nat. Clim. Chang. 11 (2), 152–157. https://doi.org/10.1038/s41558-020-00958-8.